Performance assessment comparison of variable density microchannels for mitigation of temperature non-uniformities

Jose-Luis Gonzalez-Hernandez[a], Abel Hernandez-Guerrero[a], Satish G. Kandlikar[b], Carlos Rubio-Jimenez[a], Jose-Luis Luviano-Ortiz[a]

[a] Department of Mechanical Engineering, University of Guanajuato, Guanajuato, Mexico,
[b] Department of Mechanical engineering, Rochester Institute of Technology, Rochester, NY, USA,
gonzalez.hernandez.jl@gmail.com, abel@ugto.mx, sgkeme@rit.edu,
caalruji@gail.com, j_luviano@yahoo.com.mx

Abstract:
An entropy generation analysis for a microchannel cooling layer is applied in the present work. The analysis includes the major irreversibilities inherent in the operation of a device in need of heavy cooling under typical working conditions. Results from the second law analysis are expressed by means of a single parameter introduced in this work, called the entropy generation ratio, EGR; it is shown in this work that the use of this single parameter accounting for the main irreversibilities associated to the thermal and hydraulic performances offers a sound basis for the assessment of microchannel heat sinks. The microchannel cooling layer consists of several flow passages, each incorporating a variable fin density configuration for mitigation of temperature non-uniformity. All the cases studied in this paper are simulated through a 3D numerical model. Selected geometrical parameters are varied, and its effects on the typical indicators such as overall thermal resistance and pressure drop along the device are reported; together with the entropy generation analysis results for each configuration. The results show that an optimal configuration, in terms of the minimum entropy generation rate, can be attained by properly selecting the operating conditions, as well as the values for the geometrical parameters. Providing a non-conventional approach using the parameter presented in this work could be used as a complementary tool to scrutinize and evaluate the goodness of different configurations and systems.

Keywords:
Microchannel heat sink, electronics cooling, entropy generation rate, 3D numerical model

1. Introduction

The use of microchannel cooling technologies is especially suitable for applications involving integrated circuit (IC) chips, where dissipation of high heat fluxes is required. Starting in 1975, the number of transistors within an IC chip has doubled every two years [1], leading to an abrupt increase of computational power, but inherently, to a higher rate of heat generated. In their pioneering work, Tuckerman and Pease [2] demonstrated that very high heat transfer coefficients can be achieved under low flow rates by incorporating microchannel flow passages. They dissipated 790 W from a 1 cm^2 surface with a rather high pressure drop of 214 kPa. Qu and Mudawar [3] verified numerically the ability of the Navier-Stokes and energy equations to capture the fluid flow and heat transfer characteristics of micro channel heat sinks; demonstrating the validity of the continuum approach for single phase flow problems at the micro-scale.

The major drawback related to the utilization of constant cross section (e.g. rectangular and circular) microchannel heat sinks is the high temperature variation intrinsic to the increasing thermal resistance imposed by the monotonic increase of the thermal boundary layer along the flow direction. Several researchers have overcome this issue by introducing extended surfaces;

nevertheless, the inclusion of fins implies an extra friction resistance; resulting in higher pressure drops [4, 5].

Steinke and Kandlikar [6] studied an enhanced microchannel heat exchanger with an offset strip fin configuration. Their results show that, although the pressure drop increases, enhanced microchannels lead to a better overall performance over plain microchannels. Colgan et al. [7] achieved pressure drops lower than 35 kPa while removing 400 W/cm^2 from a 20×20 mm surface through the use of optimized cooler fin designs with an offset configuration. Hong and Cheng [8] dissipated 100 W/cm^2 from the base of a 12×12 mm surface. Rubio-Jimenez et al. [9] studied microchannels with a variable fin density configuration for achieving more homogeneous temperature distributions. They considered circular, square, elliptical and flat fin geometries under a 100 W/cm^2 heat flux. For all the fin profiles analyzed, they achieved pressure drops lower than 90 kPa. Later on, the authors showed in [10] that the in-line array is over-performed by the staggered configuration, by achieving an almost 2 K lower temperature distribution than their previous work [9]. Lorenzini-Gutierrez and Kandlikar [11] numerically evaluated the cooling performance of different flow channel designs suitable for 3D IC applications. They demonstrated that microchannels with variable fin density having offset strip fins are capable to dissipate a thermal load of 200 W from a 10×10 mm 3D IC chip while maintaining uniform temperature distributions under pressure drops lower than 40 kPa.

Several researchers have implemented second law analyses to assess the overall performance of heat sinks. Lin and Lee [12] evaluated the overall performance of pin fin heat sinks with in-line and staggered configurations by incorporating the entropy generation rate (EGR) as indicator since it considers the irreversibilies related to the thermal and hydraulic performances. Results of their investigation allowed finding an optimal value of the operating conditions for the configurations studied. Khan et al.[13] evaluated the thermodynamic losses of different configurations of circular finned heat sinks by computing the EGR of the different configurations. More recently Gonzalez-Hernandez et al. [14] analyzed a pin fin heat sink with sinusoidal fin profile. They studied the effect of varying the properties of the sinusoidal function, pin fin density and operating conditions on the overall performance. They assessed the overall performance by means of the EGR. The implementation of the EGR aided the selection of the best performing configuration.

The aim of this investigation is to design a configuration capable of dissipating high heat fluxes with a low as possible pressure drop, while maintaining the surface temperature uniform and below the limit required for IC chips. The results from this investigation demonstrate that with an appropriate selection of geometrical parameters it is possible for microchannel cooling layers of 100 μm and 200 μm thick to provide cooling for a 3D IC stack for power dissipations of up to 200 W with relatively low pressure drops and highly homogeneous surface temperature distributions.

Three dimensional stacking of IC chips enables an increase of computational power per unit surface area, as compared with planar IC chips. However, a high cost must be paid for the increase of power density —the heat flux generated by the multiple stacks of IC chips leads to a dramatic increase in the peak temperature between adjacent tiers.

2. Geometry description

The microchannel cooling layer studied in this work is depicted in Figure 1. The dimensions of the base are L×W; it is subjected to a uniform heat flux *q”* at both the bottom and top surfaces. The

cooling layer consists of 12 flow channels, each with dimensions $w_c \times H$, separated by walls of thickness w_f. Values of these dimensions are summarized in Table 1.

Each of the 12 flow channels possesses a variable fin density configuration at both bottom and top walls. Figure 2 depicts the front view of a flow channel, where t_b is the thickness of the upper and lower walls, the height and width of the fins are b and t_f, respectively. All the flow channels incorporate a variable internal configuration and are divided in four regions; each region with dimensions L_r along the flow channel. The length of the fins in the flow direction is l_f. There is no gap between consecutive fins along the flow direction. The four regions considered are:

1. Region 1—rectangular smooth channel formed by flat walls.
2. Region 2—one fin region.
3. Region 3—two fins region.
4. Region 4—three fins region.

The aim of having a smooth channel configuration at the inlet (Region 1) is to attain low friction losses in the entrance region, as well as provide a more homogeneous flow distribution to the finned regions. Regions 2-4 possess an offset strip fin with variable fin density configuration that increases along the flow direction, leading to a higher heat transfer coefficient that overcomes the decrease of the temperature difference as the fluid flows through the flow channels. Offset strip fins are introduced because as stated in [6], the fluid travels in the flow direction a short distance, next the fluid encounters an obstruction and then it separates and moves around the next fin. This process is repeated as the fluid moves down the entire flow length. As a result of this, the fluid always remains in a developing state, increasing the mixing and leading to a heat transfer enhancement.

Figure 3 shows a schematic of the bottom wall of a single flow passage, where the four different regions are depicted. The configuration of the fins on the top wall corresponds to a mirror image of the fins on the bottom wall; thus a displacement exists between the fins on both walls. Figure 4 shows the fins configuration of Regions 2-4. This configuration is kept constant throughout this investigation.

Figure 1. Schematic of a microchannel cooling layer heated at both, bottom and top surfaces.

Figure 2. Front view of a single flow channel.

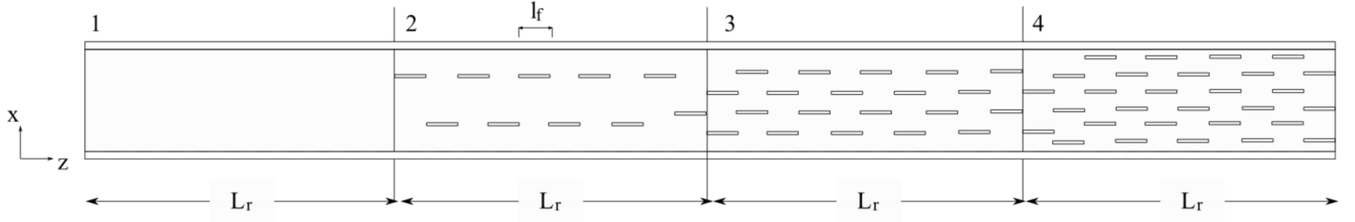

Figure 3. Schematic of the different regions along a single flow channel.

All the geometrical parameters are kept constant, except the height of the fins, *b*, and the height of flow channels, *H*. Values for these parameters are listed in Table 1. In order to maintain the aspect ratio fixed between *b* and *H* for the different configurations simulated, a non-dimensional fin height is introduced, and defined as:

$$b^* = \frac{b}{H/2} \tag{1}$$

Additional to the variable fin density flow channels, two cases corresponding to smooth rectangular channels, P1 and P2 were considered for comparison purposes. Table 2 lists the 10 different geometries considered in this study and their values of *b* and *H*.

3. Numerical model

3.1. Model assumptions

The model consists of a microchannel cooling layer with 12 flow passages. To simulate the thermal interaction between adjacent tiers of IC chips within a 3D IC, a heat flux *q*” is applied both on the top and on bottom surfaces of the cooling layer. The cooling is achieved by flowing coolant through the flow channels at a volumetric flow rate $\dot{V}$. The heat transfer mechanism consists mainly of conduction in the solid domain and forced convection in the fluid domain. In order to simplify this complex conjugate heat transfer phenomenon, the following assumptions are made:

(1) Steady state.
(2) Fully developed flow at the inlet.
(3) Constant and uniform heat flux supplied to the bottom and top surfaces.
(4) Negligible radiation heat transfer effects.
(5) Constant fluid and solid thermophysical properties, except fluid dynamic viscosity.

Numerical values for the thermophysical properties of the fluid and solid are reported in Table 3 [15–17]. For all the simulations, the coolant fluid used was water and the solid domain was regarded as silicon. The dynamic viscosity of water is determined using Equation (2):

$$\mu = 2.414\times10^{-5}\left(10^{247.8/(T-140)}\right)\mathrm{Pa\cdot s} \tag{2}$$

3.2. Governing Equations and Boundary Conditions

The conservation equations, based on the model assumptions, solved numerically for the fluid domain are: continuity, Equation (3); momentum on the x, y and z directions, Equations (4), (5) and

(6), respectively; and energy, Equation (7). For the solid domain, the energy equation reduces to Equation (8).

A constant and uniform heat flux of q''=153.186 W/cm^2 was imposed on both the bottom and top surfaces of the cooling layer. The effect of the variation of the volumetric flow rate on the cooling performance will be analyzed by considering two different volumetric flow rates evenly divided through the 12 flow channels for each configuration analyzed. The numerical values of these two volumetric flow rates are 145.53 ml/min and 72.765 ml/min (12.1275 ml/min and 6.06375 ml/min per single flow channel, respectively). The inlet temperature of the fluid was 303 K. In order to satisfy Equation (3), a mass conservation condition ($\dot{m}_{in} = \dot{m}_{out}$) was specified at the outlet of the fluid domain.

As a consequence of the uniform and constant heat flux, as well as for the homogeneous internal distribution of the volumetric flow rate, it is expected that the flow field and temperature distribution attain similar values in every flow channel. A reasonable approximation with no significant loss in accuracy was to simulate only a single flow channel; this will reduce the computation time requiredo. To achieve this, two symmetry boundary conditions were imposed at the mid-planes of the channel walls adjacent to the flow passage; the computational domain considered is equivalent to the shadowed region of Figure 1. The walls where the fluid and solid domains concur were set as interfaces with zero mass flux across them and subjected to a no-slip boundary condition. The walls adjacent to both inlet and outlet were considered as adiabatic.

A grid independency analysis was conducted for cases C1-1Y, C1-4Y and C2-1Y. The criterion for grid independency was attained when $|(N^j - N^{j+1})/N^j| < 1\times10^{-3}$. In this criterion N^j stands for the computed value of the comparison parameter and, N^{j+1} is the value obtained with the next mesh refinement. The selected comparison parameters were the pressure drop and the average temperature of the heating surface at the exit ($z=L$). Results from the grid independency analysis for the different cases are shown in Table 4. For all cases, the mesh model No. 2 ensures that the solution is grid independent; hence, all simulations are conducted by employing similar mesh sizes and distributions.

$$\frac{\partial u}{\partial x} + \frac{\partial v}{\partial y} + \frac{\partial w}{\partial z} = 0 \tag{3}$$

$$\rho_f \left(u\frac{\partial u}{\partial x} + v\frac{\partial u}{\partial y} + w\frac{\partial u}{\partial z} \right) = -\frac{\partial p}{\partial x} + \mu\nabla^2 u \tag{4}$$

$$\rho_f \left(u\frac{\partial v}{\partial x} + v\frac{\partial v}{\partial y} + w\frac{\partial v}{\partial z} \right) = -\frac{\partial p}{\partial y} + \mu\nabla^2 v \tag{5}$$

$$\rho_f \left(u\frac{\partial w}{\partial x} + v\frac{\partial w}{\partial y} + w\frac{\partial w}{\partial z} \right) = -\frac{\partial p}{\partial z} + \mu\nabla^2 w \tag{6}$$

$$\rho_f c_{\mathrm{pf}} \left(u\frac{\partial T}{\partial x} + v\frac{\partial T}{\partial y} + w\frac{\partial T}{\partial z} \right) = k_f \nabla^2 T \tag{7}$$

$$\nabla^2 T = 0 \tag{8}$$

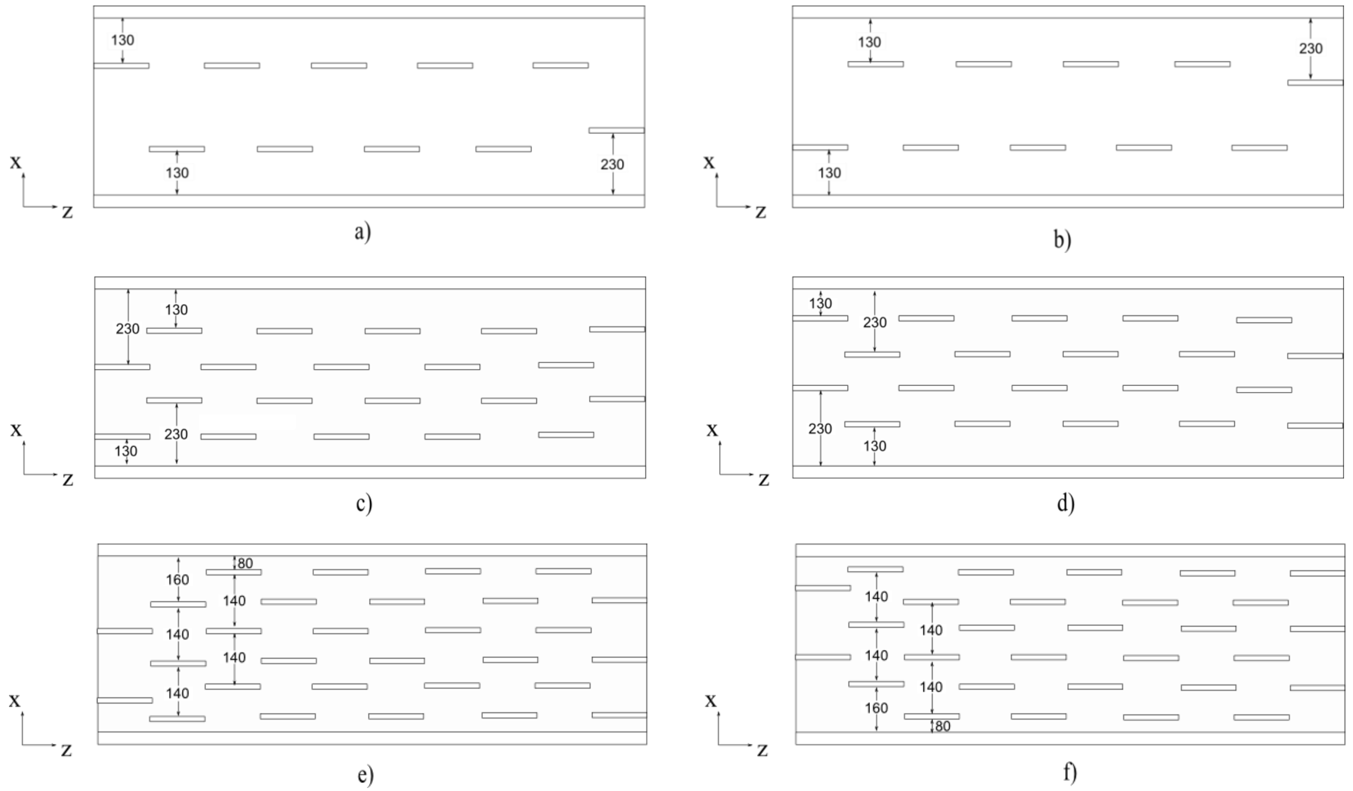

Figure 4. Fin distribution of the different regions analysed, a) Region 2, bottom wall, b) Region 2, top wall, c) Region 3, bottom wall, d) Region 3, bottom wall, e) Region 4, bottom wall, f) Region 4, top wall. Dimensions in μm.

Table 1. Values for the geometrical parameters of the flow channel.

Parameter	Symbol	Value
Length of the base (mm)	L	8
Width of the base (mm)	W	7.92
Width of the channel (μm)	w_c	560
Height of the channel (μm)	H	100, 200
Length of the fins (μm)	l_f	200
Height of the fins (μm)	b	20,30, 40, 50, 60, 80, 100
Non-dimensional height of the fins	b^*	0.4, 0.6, 0.8, 1
Width of the fins (μm)	t_f	20

Table 2. Nomenclature considered in this study.

Nomenclature	H, μm	b,μm
P1	100	0
C1-1Y	100	20
C1-2Y	100	30
C1-3Y	100	40
C1-4Y	100	50
P2	200	0
C2-1Y	200	40
C2-2Y	200	60
C2-3Y	200	80
C2-4Y	200	100

Table 3. Properties of silicon and water.

Property	Symbol	Silicon	Water
Density (kg/m3)	ρ_{si}, ρ_f	2330	998
Thermal conductivity(W/(m K))	k_{si}, k_f	148	0.6
Specific heat (J/(kg K))	c, c_{pf}	700	4182
Dynamic viscosity (Pa s)	μ	—	from Eq. (2)

Table 4. Grid independency analysis.

Case	Mesh model	Mesh elements	Δp (kPa)	$\left\lvert \frac{\Delta p^j - \Delta p^{j+1}}{\Delta p^j} \right\rvert$	$\bar{T}_{z=L}$ (K)	$\left\lvert \frac{\bar{T}^j_{z=L} - \bar{T}^{j+1}_{z=L}}{\bar{T}^j_{z=L}} \right\rvert$
C1-1Y	1	1,590,728	28.38	8.739×10^{-2}	339.98	9.677×10^{-3}
	2	2,875,950	30.86	$9.721\times^{-4}$	343.27	5.535×10^{-4}
	3	4,185,364	30.89	—	343.46	—
C2-1Y	1	1,735,452	4.86	6.790×10^{-2}	350.47	6.249×10^{-3}
	2	3,078,860	5.19	9.625×10^{-4}	352.66	3.686×10^{-4}
	3	4,596,084	5.19	—	352.79	—
C1-4Y	1	1,872,756	59.65	$6.521\times10\text{-}^{2}$	323.41	8.998×10^{-3}
	2	3,329,344	63.54	6.295×10^{-4}	326.32	2.145×10^{-4}
	3	4,681,890	63.58	—	326.39	—

4. Overall performance comparison parameters

The first indicator introduced is the thermal resistance, which is the ratio of the increment of the surface temperature above the input coolant temperature to the dissipated power. Enhanced heat transfer surfaces result in lower average surface temperatures and therefore lower thermal resistances for fixed input coolant temperature and rate of heat dissipated.

$$R = \frac{T_{s,ave} - T_{f,in}}{q'' A_s} \tag{9}$$

Together with the thermal resistance, another important indicator of the performance is the pumping power, which provides the power required to drive the coolant through the flow channels.

$$\dot{W}_p = \Delta p \dot{V} \tag{10}$$

The overall performance of the microchannel cooling layer is evaluated via the entropy generation rate evaluation.

$$\dot{S}_{gen} = \left[\frac{(q'' A_s)^2}{T_{f,in} T_{s,ave}} \right] R + \frac{\dot{W}}{T_{f,in}} \tag{11}$$

5. Results

The velocity, pressure and temperature fields were obtained numerically through the computational domains for the cases listed in Table 2. A numerical surface integration was computed for planes

parallel to the fluid inlet to assess the average values of pressure and temperature along the flow channel. As an attempt to verify the accuracy of the numerical model, the rise of fluid temperature from inlet to outlet obtained numerically was compared to that obtained from the energy balance, Equation (12). The discrepancy between numerical values and those calculated using Equation (12) was lower than 0.03% for all the cases simulated in this work. To illustrate this, consider for example case C1-1Y, the value predicted by Equation (12) is 19.756 K, while the value of ΔT_f obtained from the numerical simulation is 19.754 K, this gives a discrepancy of 0.01 %.

$$\Delta T_{\mathrm{f}} = \frac{q'' A_s}{\dot{V} \rho_{\mathrm{f}} c_{\mathrm{pf}}} \tag{12}$$

5.1 Performance assessment of the variable fin density configurations

Figure 5 shows the temperature variation of the heating surface along the flow direction for the cases incorporating a microchannel height of 100 µm. The dashed line corresponds to the maximum temperature allowable for the heating surface (80°C). The inclusion of fins with the studied configuration leads to attain lower temperatures on the heating surface, as compared to the case of a smooth channel (P1). The variation of heating surface temperature is also reduced along the finned regions (after x=2 mm) for the C1-1Y to C1-4Y cases. The surface temperature decreases as the fin height increases since more surface area is in contact with the coolant. The minimum surface temperature is achieved with the fin height of 50 µm (C1-4Y). Figure 6 depicts the variation of the heating surface along the flow channel for the cases with a microchannel height of 200 µm. The surface temperature of the P2 case is above the limit for IC chips; case C2-1Y presents a maximum surface temperature near to the allowable limit toward the exit of the flow channel; thus, under a volumetric flow rate of $\dot{V}$=145.53 ml/min these cases are not suitable for 3D IC applications. Surface temperature for C2-2Y to C2-4Y configurations are in close proximity to each other; and its values are below 340 K (67°C).

Values of the selected performance indicators are listed in Table 5. The thermal resistance is sensible to the variation of microchannel and fin heights; it decreases as the fin height increases, and increases with the channel height. By comparing the R and Δp columns, it can be observed that a trade-off exists between thermal and hydraulic performances, the minimum value of R is achieved by the C1-4Y case; however, this configuration presents the maximum pressure drop. All cases with H=200 µm present low pressure drops, but, thermal performance decreases as compared with the H=100 µm cases. The EGR parameter takes into account the irreversibilities inherent to the thermal and hydraulic performances. The minimum value of this parameter dictates the best performing configuration in terms of irreversibilies present in the performance of the device. The C1-4Y configuration presents the minimum value of the EGR. This configuration achieves the minimum value of the average surface temperature (326.5 K). The ratio $EGR/(EGR)_{plain}$ offers a direct comparison of the overall performance of the offset configurations to the case of a plain channel for a given microchannel height.

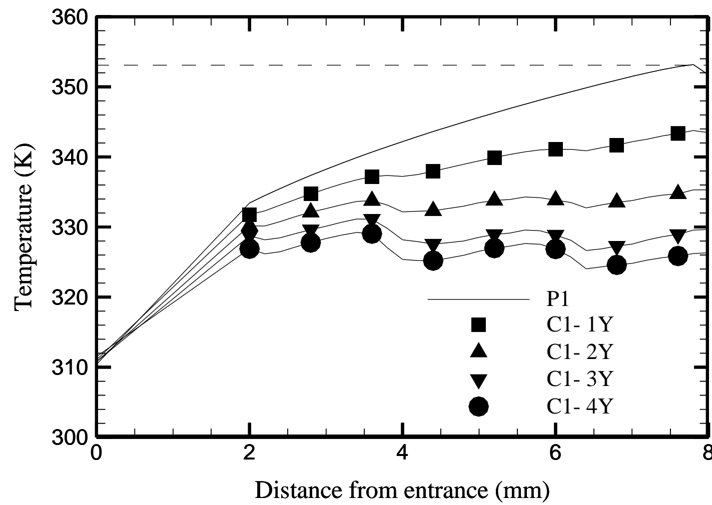

Figure 5. Surface temperature distribution for H =100 μm and $\dot{V}$ =145.53 ml/min.

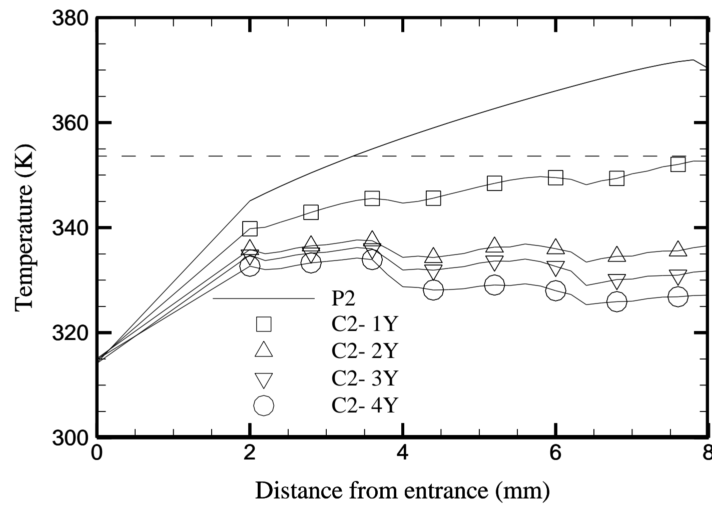

Figure 6. Surface temperature distribution for H =200 μm and $\dot{V}$ =145.53 ml/min.

5.2 Performance assessment of the variable fin density configurations — effect of the volumetric flow rate

The effect of halving $\dot{V}$ on all the studied configurations was investigated. Table 6 summarizes the values of selected parameters for the assessment of the overall performance of all configurations. Results reported in Table 6 are in agreement with the results from Table 5; nonetheless, higher values of the EGR are obtained for the volumetric flow rate of 72.765 ml/min. This implies that by operating the microchannel cooling layer with a volumetric flow rate of 145.53 ml/min the irreversibilities are reduced. The configuration presenting the best overall performance is the C1-4Y case.

Table 5. Performance indicators for volumetric flow rate of 145.53 ml/min.

Case	R (K/W)	Δp (kPa)	$\dot{W}$ (mW)	$T_{s,ave}$ (K)	$\dot{S}_{gen}$ (W/K)	$\dot{S}_{gen}/(\dot{S}_{gen})_{plain}$
P1	0.28	19.65	47.67	344.9	0.1073	1
C1-1Y	0.24	28.51	69.15	338.9	0.0937	0.8732
C1-2Y	0.21	38.47	93.30	333.2	0.0835	0.7781
C1-3Y	0.18	50.33	122.08	328.8	0.0727	0.6771
C1-4Y	0.17	63.54	154.12	326.5	0.0692	0.6452
P2	0.38	2.41	2.93	360.8	0.1390	1
C2-1Y	0.30	5.19	6.30	347.0	0.1142	0.8210
C2-2Y	0.23	8.63	10.47	335.7	0.0905	0.6507
C2-3Y	0.21	11.61	14.07	332.8	0.0833	0.5994
C2-4Y	0.19	15.40	18.67	329.3	0.0762	0.5482

Table 6. Performance indicators for the volumetric flow rate of 72.765 ml/min.

Case	R (K/W)	Δp (kPa)	$\dot{W}$ (mW)	$T_{s,ave}$ (K)	$\dot{S}_{gen}$ (W/K)	$\dot{S}_{gen}/(\dot{S}_{gen})_{plain}$
P1	0.36	8.64	20.95	358.1	0.1328	1
C1-1Y	0.33	11.67	28.3	352.1	0.1238	1.1536
C1-2Y	0.29	14.92	36.19	346.4	0.1106	1.0308
C1-3Y	0.27	18.73	45.43	342.3	0.1043	0.9716
C1-4Y	0.25	22.23	53.91	340	0.0972	0.9061
P2	0.51	1.09	1.33	379.6	0.1774	1
C2-1Y	0.42	1.95	2.36	364.5	0.1521	1.0940
C2-2Y	0.35	2.92	3.55	353.9	0.1306	0.9390
C2-3Y	0.3	4.38	5.31	345.6	0.1146	0.8243
C2-4Y	0.27	5.67	6.87	341.4	0.1044	0.7510

6. Conclusions

The overall performance of a cooling layer with offset strip fins variable fin density microchannels suitable for 3D IC applications was numerically investigated. Results from this investigation demonstrate the ability of variable fin density microchannels with offset configurations to maintain the surface below the temperature allowable limits for IC chips while presenting low pressure drops.

All the configurations studied in this work were simulated under typical operating conditions. The total thermal power applied on the cooling layer was 200 W. The effect of varying the volumetric flow rate on the overall performance for the different configurations was analyzed. Two different microchannel heights were considered, 100 µm and 200 µm. A total of 8 geometries with offset strip fins and variable fin density were modeled. Two additional cases, consisting of rectangular plain microchannels, one for each different microchannel height, were modeled to offer a reference for comparison of the overall performance.

The EGR parameter provides a criterion for selecting the best performing configuration since it includes the most important irreversibilities related to the operation of the microchannel cooling layer. The best performing configuration, in terms of the minimum value of the EGR, is the C1-4Y case. This configuration is capable of maintaining the heating surface at an average temperature of 326.5 K under a pressure drop of 63.54 kPa (pumping power of 154.12 mW) for the volumetric flow rate of 145.53 ml/min.

The effect of varying the volumetric flow rate was analyzed. All the configurations were tested under a volumetric flow rate of 72.762 ml/min. For the lower volumetric flow rate, the numerical values of the EGR parameter were increased as compared with the higher flow rate; although results exhibited a similar trend. For both operating conditions, the best performing configuration was the C1-4Y case.

7. Nomenclature

A	heat transfer area (m^2)
T	temperature, (K)
p	pressure (Pa)
c, c_p	specific heat (J kg^{-1} K^{-1})
$\dot{W}$	pumping power (W)
k	thermal conductivity (W m^{-1} K^{-1})
u, v, w	velocity components (m s^{-1})
R	thermal resistance (K W^{-1})
q''	heat flux (W m^{-2})
$\dot{V}$	volumetric flow rate (m^3 s^{-1})
H	height of the fins (μm)
L	length (μm)
W	width (μm)
L_r	length of the region (μm)
$\dot{S}_{gen}$	Entropy generation rate (W/K)
t_b	thickness of the upper and lower walls (μm)
t_f	width of the fins (μm)
b	height of the fins
w_c	width of the channel (μm)
l_f	length of the fins (μm)
w_f	width of the channel walls (μm)
b^*	non-dimensional fin height

Greek symbols

ρ	density (kg m^{-3})
μ	dynamic viscosity (Pa s)
Δp	pressure drop (Pa)

Subscripts

max	Maximum
min	Minimum
s	heating surface
f	fluid
si	silicon
ave	average
plain	plain channel

8. References

[1] G. E. Moore, "Cramming more components onto integrated circuits, Reprinted from Electronics, volume 38, number 8, April 19, 1965, pp.114 ff.," *IEEE Solid-State Circuits Newsl.*, vol. 20, no. 3, pp. 33–35, Sep. 2006.

[2] D. B. Tuckerman and R. F. W. Pease, "High-performance heat sinking for VLSI," *IEEE Electron Device Lett.*, vol. 2, no. 5, pp. 126–129, May 1981.

[3] W. Qu and I. Mudawar, "Experimental and numerical study of pressure drop and heat transfer in a single-phase micro-channel heat sink," *Int. J. Heat Mass Transf.*, vol. 45, no. 12, pp. 2549–2565, Jun. 2002.

[4] T. Kishimoto and S. Saski, “Cooling characteristics of diamond-shaped interrupted cooling fin for high-power LSI devices,” *Electron. Lett.*, vol. 23, no. 9, p. 456, 1987.
[5] Y. Peles, A. Koşar, C. Mishra, C.-J. Kuo, and B. Schneider, “Forced convective heat transfer across a pin fin micro heat sink,” *Int. J. Heat Mass Transf.*, vol. 48, no. 17, pp. 3615–3627, Aug. 2005.
[6] M. E. Steinke and S. G. Kandlikar, “Single-Phase Liquid Heat Transfer in Plain and Enhanced Microchannels,” pp. 943–951, Jan. 2006.
[7] E. G. Colgan, B. Furman, M. Gaynes, W. S. Graham, N. C. LaBianca, J. H. Magerlein, R. J. Polastre, M. B. Rothwell, R. J. Bezama, R. Choudhary, K. C. Marston, H. Toy, J. Wakil, J. A. Zitz, and R. R. Schmidt, “A Practical Implementation of Silicon Microchannel Coolers for High Power Chips,” *IEEE Trans. Compon. Packag. Technol.*, vol. 30, no. 2, pp. 218–225, Jun. 2007.
[8] F. Hong and P. Cheng, “Three dimensional numerical analyses and optimization of offset strip-fin microchannel heat sinks,” *Int. Commun. Heat Mass Transf.*, vol. 36, no. 7, pp. 651–656, Aug. 2009.
[9] C. A. Rubio-Jimenez, S. G. Kandlikar, and A. Hernandez-Guerrero, “Numerical Analysis of Novel Micro Pin Fin Heat Sink With Variable Fin Density,” *IEEE Trans. Compon. Packag. Manuf. Technol.*, vol. 2, no. 5, pp. 825–833, May 2012.
[10] C. A. Rubio-Jimenez, S. G. Kandlikar, and A. Hernandez-Guerrero, “Performance of Online and Offset Micro Pin-Fin Heat Sinks With Variable Fin Density,” *IEEE Trans. Compon. Packag. Manuf. Technol.*, vol. 3, no. 1, pp. 86–93, Jan. 2013.
[11] D. Lorenzini-Gutierrez and S. G. Kandlikar, “Variable Fin Density Flow Channels for Effective Cooling and Mitigation of Temperature Nonuniformity in Three-Dimensional Integrated Circuits,” *J. Electron. Packag.*, vol. 136, no. 2, pp. 021007–021007, Apr. 2014.
[12] W. W. Lin and D. J. Lee, “Second-law analysis on a pin-fin array under crossflow,” *Int. J. Heat Mass Transf.*, vol. 40, no. 8, pp. 1937–1945, May 1997.
[13] W. A. Khan, J. R. Culham, and M. M. Yovanovich, “Optimization of pin-fin heat sinks using entropy generation minimization,” *IEEE Trans. Compon. Packag. Technol.*, vol. 28, no. 2, pp. 247–254, Jun. 2005.
[14] J.-L. Gonzalez-Hernandez, A. Hernandez-Guerrero, C. Rubio-Jimenez, and C. Rubio-Arana, “Analysis of Pin-Fin Heat Sinks With an Unconventional Fin Profile,” presented at the ASME 2013 International Mechanical Engineering Congress and Exposition, 2013, pp. V08BT09A033–V08BT09A033.
[15] *International Steam Tables - Properties of Water and Steam based on the Industrial Formulation IAPWS-IF97*. .
[16] A. S. Okhotin, A. S. Pushkarskij, and V. V. Gorbachev, “Thermophysical properties of semiconductors,” 1972.
[17] T. Al-Shemmeri, *Engineering Fluid Mechanics*., Ventus Publishing, Holland, 2012.